Monolithic Multiband CMUTs for Photoacoustic Computed Tomography With *In Vivo* Biological Tissue Imaging

Sio Hang Pun, *Member, IEEE,* Yuanyu Yu, *Member, IEEE,* Jian Zhang, Jiujiang Wang, *Student Member, IEEE,* Ching-Hsiang Cheng, *Member, IEEE,* Kin Fong Lei, *Senior Member, IEEE,* Zhen Yuan, *Member, IEEE,* and Peng Un Mak, *Senior Member, IEEE*

***Abstract*— Among the biomedical imaging modalities, photoacoustic computed tomography (PACT) was one of the emerging hybrid techniques in recent years. In designing the PACT imaging system, a finite-bandwidth transducer is one of the limited factors for the overall performance. As the target size is inversely proportional to the dominant frequency components of the generated photoacoustic (PA) signal, a broad bandwidth transducer is desired for different scales' imaging. In this paper, a monolithic multiband capacitive micromachined ultrasonic transducer (CMUT) array was designed and fabricated for the reception of the wideband PA signals so as to provide high-resolution images with high-frequency CMUT arrays and present the high signal-to-noise-ratio major structure with low-frequency CMUT arrays. To demonstrate its performance, a phantom experiment was conducted to show and evaluate the various qualities of multiresolution images. In addition, an *in vivo* mouse model experiment was also carried out for revealing the multiscale PA imaging capability with the multiband CMUTs on biological tissues. From the obtained results, the images from different CMUT arrays could show the structures of the mouse brain in different scales. In addition, the images from the high-frequency CMUT arrays were able to reveal the major blood vasculatures, whereas the images from low-frequency CMUT arrays showed the gross macroscopic anatomy of the brain with higher contrast.**

***Index Terms*— Capacitive micromachined ultrasonic transducer (CMUT), multiband CMUT, photoacoustic computed tomography (PACT).**

Manuscript received July 26, 2017; accepted January 8, 2018. Date of publication January 12, 2018; date of current version March 1, 2018. This work was supported in part by the Science and Technology Development Fund of Macau (FDCT) under Grant 087/2012/A3, Grant 047/2013/A2, Grant 093/2015/A3, Grant 088/2016/A2, Grant 026/2014/A1, and Grant 025/2015/A1, and in part by the Research Committee of the University of Macau under Grant MYRG2014-00010-AMSV, Grant MYRG2015-00178-AMSV, Grant MYRG2016-00157-AMSV, Grant MYRG079(Y1-L2)-FST12-VMI, Grant MYRG103(Y1-L3)-FST13-VMI, Grant MYRG2014-00093-FHS, Grant MYRG2015-00036-FHS, and Grant MYRG2016-00110-FHS. *(Corresponding authors: Yuanyu Yu; Zhen Yuan.)*

S. H. Pun is with the State Key Laboratory of Analog and Mixed-Signal VLSI, University of Macau, Macau 999078, China.

Y. Yu was with the State Key Laboratory of Analog and Mixed-Signal VLSI, University of Macau, Macau 999078, China, and also with the Department of Electrical and Computer Engineering, Faculty of Science and Technology, University of Macau, Macau 999078, China. He is now with the School of Information Engineering, Lingnan Normal University, Zhanjiang 524048, China (e-mail: yuyuanyu@gmail.com).

J. Zhang was with the Bioimaging Core, Faculty of Health Sciences, University of Macau, Macau 999078, China. He is now with the Department of Biomedical Engineering, Guangzhou Medical University, Guangzhou 510182, China.

J. Wang is with the State Key Laboratory of Analog and Mixed-Signal VLSI, University of Macau, Macau 999078, China, and also with the Department of Electrical and Computer Engineering, Faculty of Science and Technology, University of Macau, Macau 999078, China.

C.-H. Cheng was with the Department of Industrial and Systems Engineering, The Hong Kong Polytechnic University, Hong Kong. He is now with the School of Automotive Engineering, Wuhan University of Technology, Wuhan 430070, China.

K. F. Lei is with the Graduate Institute of Medical Mechatronics, Chang Gung University, Taoyuan 33302, Taiwan, and also with the Department of Radiation Oncology, Chang Gung Memorial Hospital, Taoyuan 33305, Taiwan.

Z. Yuan is with the Bioimaging Core, Faculty of Health Sciences, University of Macau, Macau 999078, China (e-mail: zhenyuan@umac.mo).

P. U. Mak is with the Department of Electrical and Computer Engineering, Faculty of Science and Technology, University of Macau, Macau 999078, China.

Digital Object Identifier 10.1109/TUFFC.2018.2792784

I. Introduction

In THE medical area, imaging is both an important diagnostic modality in clinical assessment and an effective aid to therapeutic treatment. With the rapid development of imaging technology over a century, nowadays, numerous imaging methodologies have been implemented and the imaging techniques have profoundly altered the medical arena. Among the available imaging techniques, photoacoustic computed tomography (PACT) is an emerging hybrid imaging technique that can reconstruct both the structural and functional information of biological tissues with high resolution, high contrast, and satisfactory penetration depth. PACT has been applied in breast cancer diagnosis, brain structure imaging, and small animal imaging [1], [2].

PACT is an imaging technology based on the photoacoustic (PA) effect. With short-pulsed laser excitations, part of the photoenergy is absorbed by the target biological tissue in accordance with the absorption property of the tissue with respect to the wavelength of the laser. When the optical excitation satisfying both thermal and stress requirements of the PA effect, the absorbed photoenergy causes a local transient thermoelastic expansion, which correlates with the thermal diffusivity, thermal expansion coefficient, and the elastic properties of the sample, and as a result, an acoustic wave/stress wave is generated [1], [3].

Based on a small light absorbing sphere [3]–[5], the corresponding PA signal generally has an "N"-shaped profile and the PA pulse duration τ_a and the half-power frequency range of the PA signal f_{lower} to f_{upper} are given by the following

equations [4]:

$$\tau_a = \frac{2a}{c} \tag{1}$$

$$f_{\text{lower}} = \frac{0.16c}{a}, \quad f_{\text{upper}} = \frac{0.51c}{a} \tag{2}$$

where c represents the propagating velocity of the acoustic wave and a depicts the diameter of the target sphere.

From (2), the frequency range of the PA signal is inversely proportional to the dimension of the sphere, i.e., higher frequency PA signal is anticipated for a sphere with smaller radius [3], [4]. Propagating from its source, the PA signal is equivalent to the traveling of ultrasonic wave in the medium where the attenuation is increased with frequency [1]. Then, the PA signal is detected by using an ultrasonic detector that can be selected from piezoelectric-based transducers [6], [7], capacitive micromachined ultrasonic transducer (CMUT) [8], and optical methods [9]–[11]. To construct an image with the PA signals, PACT combines multiple PA signals received from angles surrounding the objects [12], [13] or from a transducer array [3]. To improve the imaging quality as well as the performance of the overall acquisition process of the PACT, numerous developments such as universal back-projection algorithm [14], delay-and-sum beam forming algorithm [12], [13], exact numerical reconstruction algorithm [15], 3-D reconstruction algorithm based on the focal-line concept [16], Neumann series-based algorithm [17], and gradient-based bound-constrained split Bregman method for large-scale 3-D reconstructions [18] were major reconstruction algorithms in the literature published recent years.

Among various ultrasonic transducers for detection of the PA signal, as mentioned in [8] and [19], the use of CMUT as a PA signal detector has several advantages, such as wider bandwidth and different sizes can be easily fabricated by using the silicon micromachining technology [20], better matching of acoustic impedance to the human body [21], easier to form ring-type/2-D arrays [22], and facile integration with front-end electronics [20].

From the literature, attempts have been made to demonstrate the capabilities of using CMUTs for PA imaging and new designs were reported for improving the PA imaging system design and quality. For example, Wygant *et al*. [23], Vaithilingam *et al*. [8], [24], [25], and Chee *et al*. [26] focused on effective scanning for the volumetric PA imaging using 2-D CMUT arrays. In terms of imaging quality improvement, integration of front-end electronics by using the flip-chip bonding technique [8], [23]–[25], [27], [28] and wide bandwidth CMUTs are the popular choices [27], [28]. More specifically, Ma *et al*. [27] and Kothapalli *et al*. [28] used a 5.5-MHz CMUT array, which was integrated with front-end electronics and had a 6-dB fractional bandwidth above 100%, to achieve 35-dB signal-to-noise ratio (SNR) PA image at 5-cm depth. Miniaturization for the PA imaging system is one of the main trends to use CMUT for the PA imaging system. Up to date, Chen *et al*. [29] proposed an infrared transparent silicon CMUT array to miniaturize the PA imager head, and Cheng *et al*. [19] fabricated a CMUT array with suitable electrically isolation for minimally invasive PA imaging applications [19]. Chee *et al*. [30] reported a dual-frequency CMUT array, and Zhang *et al*. [31] also published a dual-band CMUT array on for higher integration of the PA system. Recently, Asao *et al*. [32] proposed their CMUT-based PA mammography simultaneously acquiring both PA and ultrasound images. Further to the technological observation, the authors also witnessed various imaging targets with CMUT from the literature and the major samples were phantoms with fishing lines [8], human hairs [26], [30], and horse hairs [27], [28]. For biological experiments with CMUT-based PA imaging system, Vaithilingam *et al.* [8] and Vaithilingam *et al.* [24] used the pig blood phantom embedded inside chick breast tissue for investigation. Lately, Zhang *et al.* [31] and Asao *et al.* [32] advanced the PACT imaging experiments on zebrafish and human subjects.

To improve the imaging quality of the PACT based on the CMUT technology, in this paper, a new monolithic multiband CMUT for PACT is proposed. By fabricating five CMUT arrays with different dimensions on the same die, the proposed CMUT arrays, whose resonance centered at different frequencies, cover a wide range of bandwidth, from 1.8 to 10.6 MHz. According to [7] and [33], a wide bandwidth ultrasonic detector can improve the quality of the PA image, whereas high-frequency components of the PA can resolve better details of the small structure (higher resolution) and the low-frequency components give the major structure with stronger signal strength (higher contrast).

The basics of the PACT and a brief review of CMUT applied in the PACT were introduced in this section. The design of the CMUT and the characterization of the fabricated CMUT arrays will be discussed in Section II. In Section III, the configuration of the PACT imaging system and the detail technique regarding the PA measurement will be given. The obtained experimental results from phantom and *in vivo* mouse model and the corresponding discussion can be found in Section IV. To wrap up, the conclusion regarding the reported work is drawn in Section V.

II. Design and Implementation

A. Design of the Multiband CMUT Arrays

The motivations behind the design of these monolithic multiband CMUT arrays are mainly based on the properties of the PA signal that higher frequency components are generally used to resolve small target feature, whereas low-frequency components are less attenuated and thus give higher contrast image. In addition, the small target absorbs less optical energy in comparison with the large one with the same absorptivity. Therefore, a wide bandwidth detector for the PA signal would be beneficial for imaging of heterogeneous targets, e.g., biological tissues.

However, it would be a challenging task to fabricate a specific dimension CMUT with extensively wide bandwidth as this CMUT requires carefully balanced optimization among several design parameters including the membrane thickness, density of membrane material, radiation impedance, and the fill factor. In addition, a wideband CMUT inevitability suffers from low mechanical quality factor, Q, as the fractional

bandwidth of a transducer is inversely proportional to Q [34]; in the meanwhile, a wide bandwidth is usually achieved at the expense of lower reception sensitivity. According to [35] and [36], the 6-dB fractional bandwidth of CMUT is generally less than 150%. Therefore, in this paper, by using multiple-frequency CMUTs to extend the bandwidth and similar to Chee *et al.* [30], the authors proposed to use five CMUT arrays with different frequencies, which were fabricated on the same die, for PA signal reception with extended bandwidth from 1.8 to 10.6 MHz. In such a way, the form factor of the CMUT arrays is kept, while the detecting capability for the PA signal can be enhanced. For the sake of completeness, it is worth mentioning that the current methodology has deficiencies including heterogeneous power system for our multiband CMUT cells, more complexity in PA signal acquisition, and long time required for PA signal acquisition.

For a circular CMUT immersed in liquid, the damped resonant frequency (angular frequency) of a membrane (f_r), provided that the membrane geometry is much smaller than acoustic wavelength, can be evaluated by using the following equation [37]:

$$f_r = \frac{\frac{2.98h}{r^2}\sqrt{\frac{E}{\rho_p\ (1-\sigma^2)}}}{\sqrt{1+0.67\frac{\rho_l r}{\rho_p h}}} \tag{3}$$

where h represents the thickness of the CMUT membrane, r is the radius of the membrane, E depicts Young's modulus of the membrane, ρ_p is the density of the membrane, σ is Poisson's ratio of the membrane, and ρ_l depicts the density of the liquid.

For the multiband CMUT arrays, in accordance with (3), the resonant frequencies of CMUT arrays can be determined by the thicknesses and radii of the membranes with all CMUT elements fabricated on the same die. However, the thicknesses of the membranes for all the CMUT cells will be similar to the membranes are formed by using the low-pressure chemical vapor deposition (LPCVD) process. In such a way, the resonant frequencies of the CMUT arrays can only be set by changing the radii of the membranes. In consideration of the material properties of the membrane, which is low-stress silicon nitride with $E \approx 220$ GPa, $\sigma \approx 0.263$, and $\rho_p \approx 3270$ kg/m^3, the properties of soybean oil ($\rho_l \approx 930$ kg/m^3) [38] and 450 nm thick of the membrane, the membrane radii should be in the range of 9–18 μm for working frequency from 2 to 10 MHz by using (3) and ought to avoid the fraction of micrometers.

Further to the initial design for determining the dimension of the multiband CMUT arrays, finite-element analysis (FEA) with the commercial package COMSOL Multiphysics 4.4 (COMSOL Inc., Stockholm, Sweden) was used to investigate the center frequencies of the immersed CMUTs. For each type of CMUT cells, a 2-D axisymmetric model was built to represent the CMUT with a bottom electrode, insulator, vacuum gap, membrane, and top electrode. In the FEA model, a cylindrical waveguide above the device was introduced for simulating the surrounding medium [39]. Its width was set to half of the CMUT cell pitch (i.e., 32 μm), and its height was equal to one wavelength of the working frequency. On the top of it, an absorbing boundary was applied to represent the medium extended to infinite space and no reflected wave bounced back from its boundary. In this paper, five FEA models with various dimensions were built and one of them (membrane radius: 11 μm) is shown in Fig. 1 for reference.

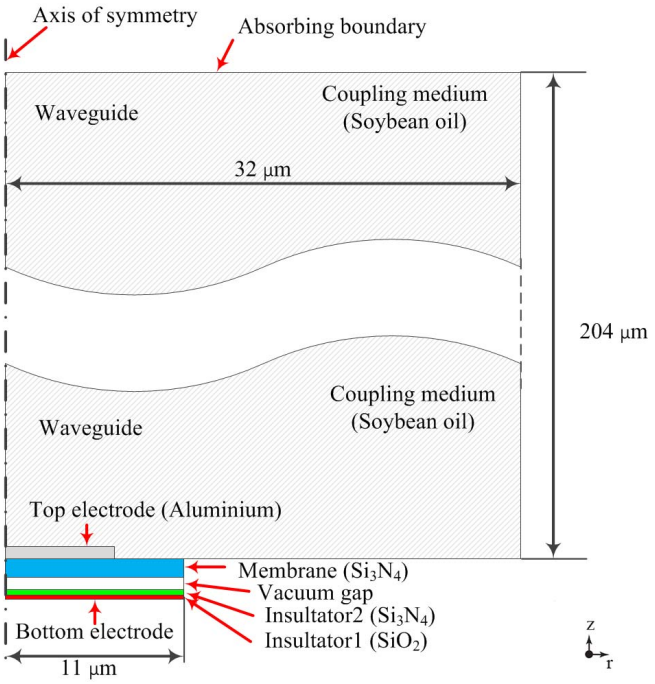

Fig. 1. Two-dimensional axisymmetric FEA model of the CMUT design with a membrane radius of 11 μm. Please note that the figure is drawn in scale.

TABLE I
PHYSICAL PARAMETERS OF THE CMUT

Number of elements in the arrays	10
Length of an element, μm	11,800
Width of an element, μm	880
Cell radius range, μm	10, 11, 13, 15, 17
Top electrode thickness, μm	0.30
Membrane thickness, μm	0.45
Cavity height, μm	0.30
Insulator (Si_3N_4) thickness, μm	0.15
Insulator (SiO_2) thickness, μm	0.10

In the simulation, the electromechanics (*emi*) and pressure acoustic (*acpr*) modules were coupled and the output pressure of the CMUT cell was calculated by averaging along the interface between the membrane and the medium with the prestressed analysis. During the analysis, each CMUT was biased with 85% of its collapsed voltage and then an AC voltage was applied to the membrane. After simulations were performed, five types of CMUTs were fabricated with the dimension as listed in Table I. Geometrically, each type of CMUT cells is arranged into two elements next to each other forming one CMUT array and the pitch of CMUT cells is 64 μm. In such a way, there are ten elements of CMUT on the die and the arrangement of the multiband CMUT arrays is illustrated in Fig. 2(a). The estimated center frequencies of five CMUT arrays were 2.8, 3.7, 5.1, 7.3, and 9.4 MHz.

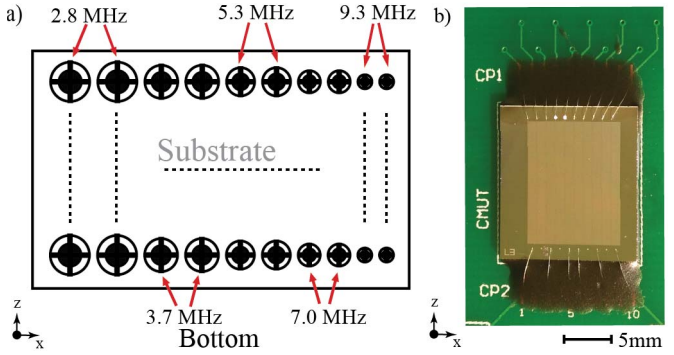

Fig. 2. (a) Arrangement and orientation of the CMUT arrays on the substrate. Different bands of CMUT arrays are arranged in perpendicular to the surface of the rotating stage. Please note that the picture is not drawn in scale. (b) Photograph of the die containing the multiband CMUT arrays, and the die is bonded on a PCB.

B. Fabrication of the Multiband CMUT Arrays

The CMUT arrays were fabricated on an n-type highly doped 4-in silicon wafer <100> using a standard sacrificial-release process with five masks [40]. At the beginning, a combined layer of 100-nm silicon oxide by using the dry oxidation process and 150-nm low-stress silicon nitride by the LPCVD process were then formed on the wafer as an insulator. Next, a 300-nm polysilicon film was deposited on the insulator by the LPCVD process to serve as a sacrificial layer. Afterward, CMUT cells with various dimensions and release channels were patterned by photolithography with Mask #1 and reactive ion etching (RIE) was performed to remove the exposed polysilicon and stop at the insulator. After removing the residual photoresist, the whole wafer was coated with a low-stress LPCVD silicon nitride layer with a thickness of 450 nm to create the membrane layer and the support structures of the CMUT cells.

At each release channel, an etch hole with a diameter of 2 μm was first patterned by photolithography with Mask #2 and was etched with the RIE process. To form the cavity under the membrane of CMUT, the wafer was immersed in 22.5 wt% KOH solution and the polysilicon under the membrane was etched via the etch holes and channels.

After creating the cavity, a KOH decontamination process was carried out, followed by a plasma-enhanced chemical vapor deposition (PEVCD) process growing a 1.2-μm silicon nitride layer to seal the etch holes. Due to the low-pressure operation of the PEVCD, the cavity of the CMUT was vacuum sealed and the CMUT became suitable for immersed operation. To restore the membrane to its designated thickness, an additional RIE was used to etch back the silicon nitride grown by the preceding PECVD process with Mask #3 to protect the sealed holes.

Next, Mask #4 was used with photolithography and RIE processes to expose the doped silicon substrate (bottom electrode of the CMUT) and a 300-nm aluminium layer was deposited by using the thermal evaporation. On the aluminium layer, the photolithography based on Mask #5 and the high-density plasma RIE (HDP-RIE) were performed in turns to form the top electrodes, bonding pads, and the interconnections for the CMUT arrays. Finally, the residual photoresist on the aluminium was cleaned by oxygen plasmas with HDP-RIE for wire bonding.

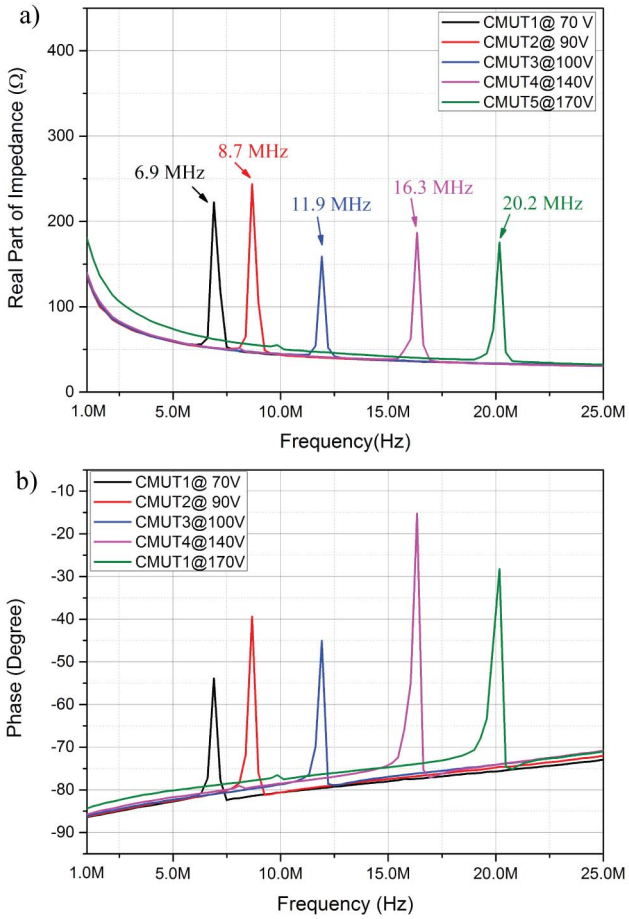

Fig. 3. Measured electrical characteristics of the five CMUT elements in air. (a) Real part of the impedances of the CMUT elements. (b) Phase plot of the impedance of CMUT elements.

The orientation and arrangement of the multiband CMUT arrays are illustrated in Fig. 2(a), while the photograph of the CMUTs die bonded on a printed circuit board (PCB) is shown in Fig. 2(b).

C. Measurements of the Multiband CMUT Arrays

The electrical characteristics of the multiband CMUT arrays in air were measured with a network/spectrum/impedance analyzer (Model: 4395A, Agilent Technologies Inc., USA) and a programmable DC power supply (Model: HSPY-400-01, Beijing HanShengPuYuan Technology Co., Ltd., China). Prior to the measurement, the analyzer was properly calibrated. Fig. 3 shows the measured impedance and phase plots for the five CMUT elements. As indicated in Fig. 3, the resonant frequencies of the five DC-biased CMUT arrays in air are 6.9, 8.7, 11.9, 16.3, and 20.2 MHz, respectively.

To further characterize the multiband CMUT arrays, the standard pulse-echo measurements for the CMUT arrays in soybean oil were performed with an output DC power supply (Model: U8031A, Agilent Technologies Inc., USA),

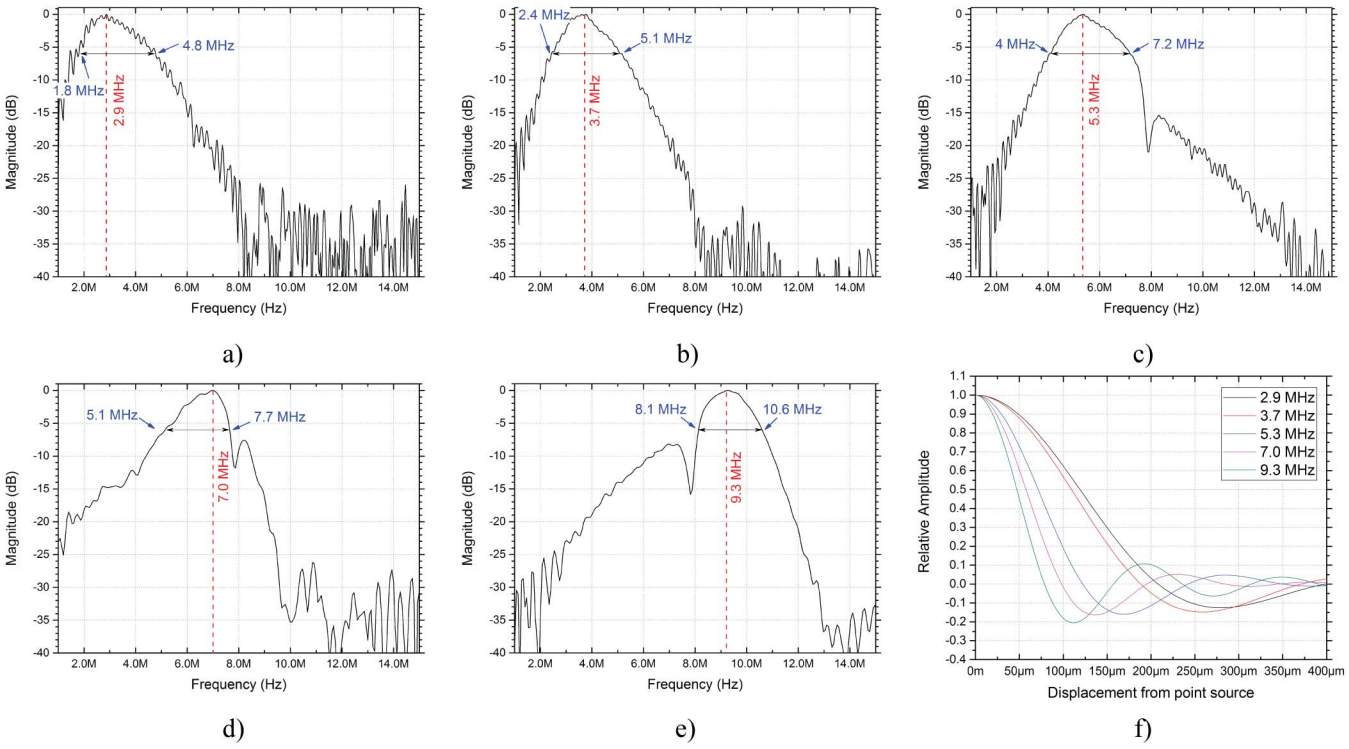

Fig. 4. Normalized 6-dB bandwidth for the fabricated multiband CMUT arrays by using the pulse-echo measurement in soybean oil. The measured center frequencies of the CMUT arrays were (a) 2.9, (b) 3.7, (c) 5.3, (d) 7, and (e) 9.3 MHz with 6-dB bandwidth of (a) 3, (b) 2.7, (c) 3.2, (d) 2.6, and (e) 2.5 MHz. (f) Theoretical PSF by the CMUT arrays based on the pulse-echo measurement result.

a programmable DC power supply (Model: HSPY-400-01, Beijing HanShengPuYuan Technology Co., Ltd., China), two waveform generators (Model: 33500B series, Keysight Technologies Inc., USA), a digital oscilloscope (Model: DSOS254A, Keysight Technologies Inc., USA), and a homemade trans-impedance amplifier circuit (Gain: 39- and 3-dB and bandwidth: 1 kHz-23 MHz) mainly consists of an operational amplifier (Model: OPA657, Texas Instruments, USA) and a protection switch (Model: ADG5419, Analog Device, USA). As shown in Fig. 4(a)–(e), the frequency responses (normalized magnitude) of the five CMUT arrays on the same die are plotted. From Fig. 4(a)–(e), the center frequencies of the CMUT arrays locate at 2.9, 3.7, 5.3, 7, and 9.3 MHz having the 6-dB bandwidth of 3, 2.7, 3.2, 2.6, and 2.5 MHz, respectively. The joint response of all the CMUT arrays can cover a wide range of acoustic waves frequencies (from 1.8 to 10.6 MHz). In addition, from Fig. 4(c)–(e), a frequency droop around 7.8 MHz was observed. According to [41] and [42], this is mainly due to the substrate ringing phenomenon at the substrate resonance frequency which is inversely proportional to the thickness of the substrate. In this design, the substrate thickness of the fabricated CMUT arrays is 525 ± 25 μm corresponding to a frequency droop at 8.1 ± 0.4 MHz theoretically.

As widely discussed in [7], the qualities of the PACT images are affected by the convolution of the optical structure of the target, profile of the laser excitation, and the impulse response of the detector. For an ideal absorption point target with infinite small size, the frequency spectrum of the PA signal has a constant power spectral density across the whole frequency range. With band-limited PA signal detectors, the reconstructed target in an image can be anticipated to have a finite diameter, which is inversely proportional to the center frequency and the frequency band of the detector. For this imaging paradigm, Xu and Wang [43] reported an analytical formulation for estimating the point spread function (PSF) resulted from band-limited detector as follows:

$$\mathrm{PSF}(R) = \frac{k_{\mathrm{Hc}}^3}{2\pi^2}\frac{j_1(k_{\mathrm{Hc}}R)}{k_{\mathrm{Hc}}R} - \frac{k_{\mathrm{Lc}}^3}{2\pi^2}\frac{j_1(k_{\mathrm{Lc}}R)}{k_{\mathrm{Lc}}R} \tag{4}$$

$$k_{\mathrm{Hc}} = \frac{2\pi f_{\mathrm{Hc}}}{c} \quad , \quad k_{\mathrm{Lc}} = \frac{2\pi f_{\mathrm{Lc}}}{c} \tag{5}$$

where f_{Lc} and f_{Hc} are the low and high cutoff frequencies of the PA signal detector, c is the speed of sound, R represents the displacement from the point source, and j_1 is the spherical Bessel function of the first kind.

In Fig. 4(f), the corresponding PSFs for the five CMUT arrays are shown. It can be found that the PSF is becoming narrow (i.e., approaching to the ideal point source) with increasing frequency of the CMUT arrays. Thus, high-frequency CMUT array is necessary for small target imaging. On the contrary, for a large-size target, the high-frequency CMUT array is generally incapable of picking up low-frequency PA signal and this results in significant artifacts in the reconstructed image [7]. Therefore, our proposed monolithic multiband CMUT arrays can be used to image for extended range of targets.

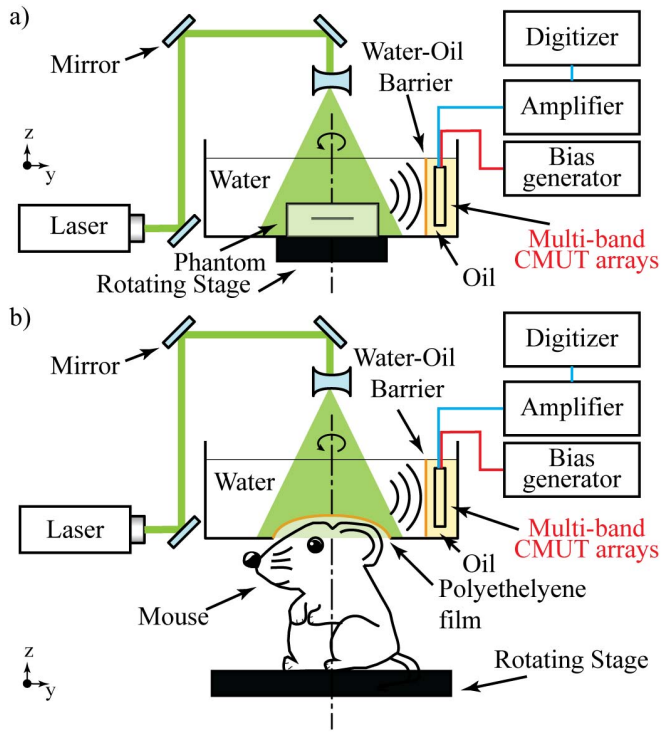

Fig. 5. (a) Configuration of the custom built PACT imaging system. The proposed multiband CMUT arrays are placed next to the biological sample, and they are immersed in soybean oil in a separate container to provide suitable electrical isolation between CMUT electrodes. (b) Configuration for imaging the brain of the mouse *in vivo*.

III. Experimental Setup

To test for the performance of the multiband CMUT arrays, a PACT imaging system was built. As shown in Fig. 5(a), a phantom was immersed in a tank, which was fixed on a motorized rotating stage (Model: X-RST120AK-E03, Zaber Technologies Inc., Canada). Alternatively, for performing the *in vivo* imaging on the mouse, a hole with a diameter of 30 mm was opened at the bottom of the water tank and it was covered with a ∼50-μm-thick transparent polyethylene film (low absorption coefficient for the current laser excitation) to isolate the tank water from the imaging target. The experimental mouse was situated on the motorized rotating stage as shown in Fig. 5(b).

In this configuration, the laser light source was an optical parametric oscillator (Model: Surelite II-20, Continuum Co., USA) generating laser at 532-nm wavelength with a repetition rate of 20 Hz and ∼5 ns in duration. Several mirrors were used to adjust the direction of the laser beam and a concave lens was employed to reshape the laser beam, so that the biological tissue was irradiated from its top (z-axis) direction and was covered completely by the laser beam. During the experiment, the optical fluence was kept below 10 mJ/cm^2 fulfilling the safety limit of 20 mJ/cm^2 prescribed by the American National Standards Institute [44]. In the current setup, the monolithic multiband CMUT arrays were placed next to the biological sample.

In contrast to the pioneering works of using CMUT in PA applications, in which vegetable oil was used as coupling material in the experiments [8], [30], the biological samples

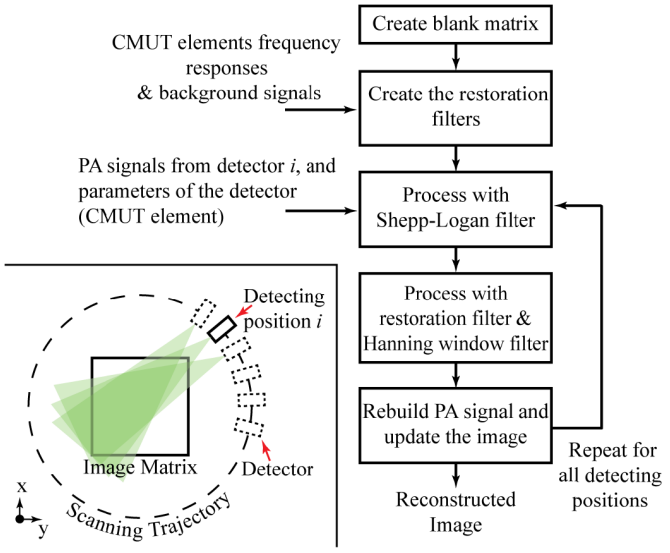

Fig. 6. Block diagram of the back-projection algorithm for the image reconstructions. The inlet exhibits the relative scanning position i for the image reconstruction.

were immersed in water in the current experiments. Comparing soybean oil and water as coupling material for the PA applications, in general, water is a better choice as its absorption coefficient is much less for laser light wavelength below 570 nm [45]. As a result, the background noise generated by the coupling medium is less. In addition, current multiband CMUT arrays have no passivation layer on their tops and operate with high applied DC bias voltages to the CMUT arrays. Therefore, a polyethylene container with a thickness of ∼50 μm was used to accommodate soybean oil as a second coupling material for the CMUT arrays to provide suitable electrical insulation. This arrangement can be considered as the PA signal traveling through a three-layered medium (water–polyethylene–soybean oil) to reach the CMUT arrays. Assuming that the PA signal is a plane wave incident on to the medium in the normal direction, the transmission coefficient T_i of the PA signal through the medium can be given by the following equation [46]:

$$T_i = \frac{4}{2 + \left(\frac{Z_3}{Z_1} + \frac{Z_1}{Z_3}\right)\cos^2 k_2 L + \left(\frac{Z_2^2}{Z_1 Z_3} + \frac{Z_1 Z_3}{Z_2^2}\right)\sin^2 k_2 L} \tag{6}$$

where Z_1, Z_2, and Z_3 are the specific acoustic impedances of water, polyethylene, and soybean oil, respectively. $k_2 = (\omega/c_2)$ is the wave number in polyethylene, ω depicts the angular frequency, c_2 represents the acoustic velocity in polyethylene, and L corresponds to the thickness of polyethylene.

In the current experimental setup, with the acoustic impedances of water ($Z_1 = 1.48$ MRayl), polyethylene ($Z_2 = 1.794$ MRayl), and soybean oil ($Z_3 = 1.346$ MRayl) [38], [47], the overall intensity transmission coefficient of the PA signal from 1 to 15 MHz is changed from 0.996 to 0.942 by (6). From the calculation, it can be found that the proposed method only introduces slight attenuation to the PA signal.

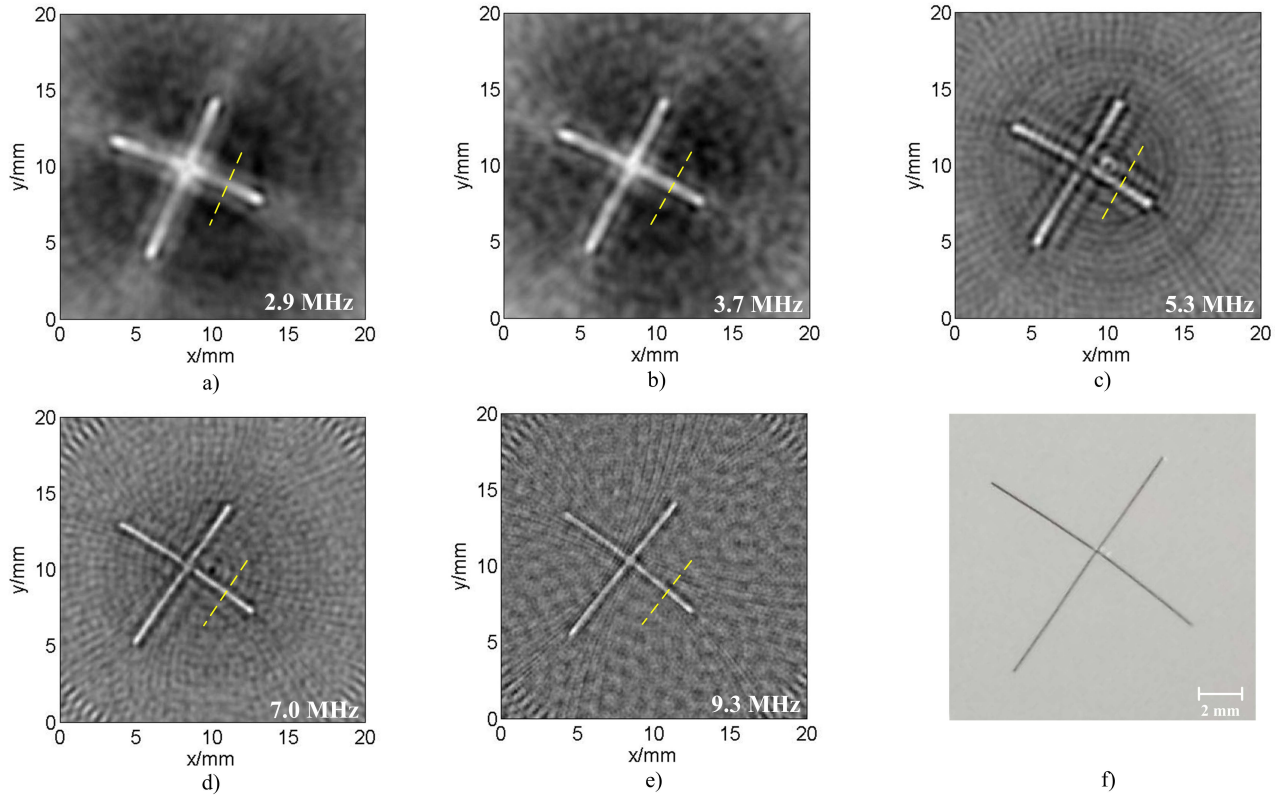

Fig. 7. Pact images of the phantom experiment using the custom built PACT imaging system. The images were reconstructed from the signal received by the CMUT arrays whose resonance frequencies at (a) 2.9, (b) 3.7, (c) 5.3, (d) 7, and (e) 9.3 MHz. (f) Photograph of the phantom with two human hairs at its center. The signal amplitudes are sampled along the yellow lines shown in Fig. 8.

In the current experimental configuration, the multiband CMUT arrays were fixed with supporting rods and were placed next to the sample. For each element of CMUT arrays, a DC bias was supplied by a programmable DC power supply (Model: HSPY-400-01, Beijing HanShengPuYuan Technology Co. Ltd., China) with 85% of its collapse voltage and the acquired PA signals were amplified by a 20-dB preamplifier (Model: Preamp2, Ultratec, Inc., USA), a 39-dB amplifier (Model: 5073PR, Olympus Co., Japan), and digitized with a data acquisition card (Model: PXI-5124, National Instruments Co., USA) at 100 MSamples/s.

During the imaging process, a Labview program was used to control the scanning and data acquisition in the system. To acquire the PA signal for reconstruction of the tomographic image, the sample was scanned for a full revolution in 120 steps. In each scanning position, the received PA signal was averaged from 40 measurements for each CMUT element. Upon the completion of the PA signal acquisitions, a back-projection algorithm [14] implemented on MATLAB was used to reconstruct the tomographic images of the biological sample based on the cylindrical geometry. With the frequency responses of the CMUT elements, detecting positions, acceptance angles of the CMUT elements, the PA signal restoration filters, Shepp–Logan filters, and Hanning window filters, the image reconstruction algorithm rebuilt the five PA images with all scanning positions for each CMUT element in turns. Fig. 6 illustrates the block diagram of the back-projection algorithm employed for the images reconstruction.

With the PACT imaging system, both phantom and *in vivo* biological experiments were designed and conducted to manifest its performances. The total time required for the PA signal acquisition and image reconstruction was about 20 min and 30 s. In these experiments, the configuration of the PACT imaging system was the same except for the biological experiment, the mouse was placed beneath the water tank with its head aligned with the open hole on the bottom of the tank.

IV. Experimental Results and Discussion

A. PACT With Phantoms

In the first phantom experiment, two human hairs with diameters of around 100 μm were anchored inside a cylindrical phantom as shown in Fig. 7(f). The composition of the phantom consists of intralipid (scatter), India ink (absorber), and agar powder (1%–2%) for solidifying the solution. Except for the human hairs, the background absorption coefficient and reduced scattering coefficients are 0.01 and 1 mm^{-1}.

As shown in Fig. 7(a)–(e), the images of the phantoms were reconstructed by using the PA signal detected from five CMUT arrays. In general, all reconstructed images were able to capture the pattern of the two human hairs in phantom. However, the obtained images were slightly different with CMUT arrays in quality. The sizes of the hairs in the reconstructed images of high-frequency band CMUT arrays (e.g., CMUT arrays centered at 7 and 9.3 MHz) were closer to the physical size than those obtained from low-frequency band CMUT arrays (e.g., 2.9 and 3.7 MHz). These

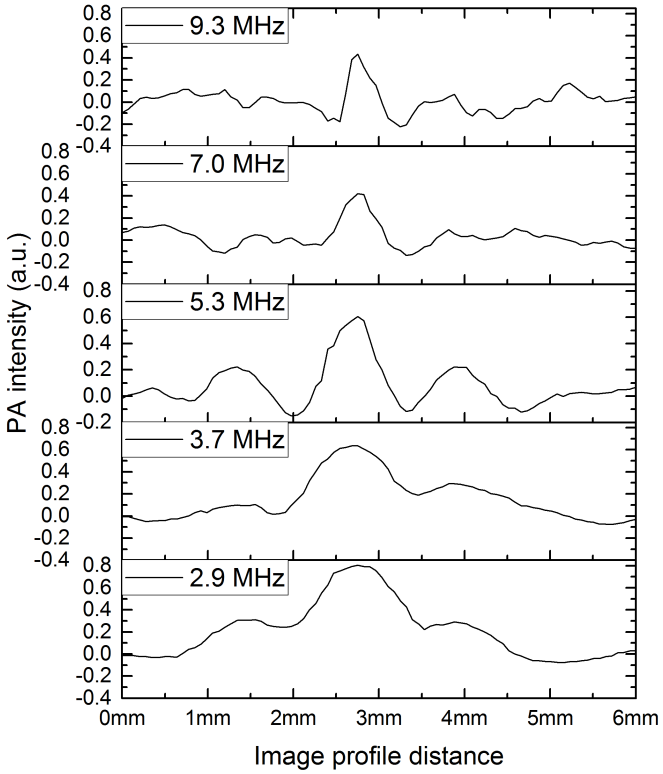

Fig. 8. Amplitude of the signals sampled from the acquired images along the yellow dash lines shown in Fig. 7(a)–(e).

matched with the theoretical investigation of the CMUT arrays for the PA signal detection discussed previously. Quantitatively, Fig. 8 also shows the image amplitude sampled along the yellow dashed lines shown in Fig. 7(a)–(e). In Fig. 7(a)–(e), it could be found that the lower frequency CMUT arrays (e.g., 2.9 and 3.7 MHz) generally have a higher amplitude in comparison with the high-frequency arrays. In addition, from the reconstructed images, the averaged signal amplitudes inside a cross mark similar to size of the hairs were measured [30] and the SNR of the images from CMUT arrays is plotted in Fig. 9. One can find that the SNR is generally higher for images from low-frequency arrays, and it is inversely proportional to the frequency of the CMUT arrays.

From the phantom experiment, one can find that the proposed monolithic multiband CMUT arrays can provide enhanced performance for the PACT. First, using the proposed multiband CMUT arrays, the PACT system can resolve details of small structure and give major structure with high SNR in the absence of sophisticated broadband ultrasonic detectors. Moreover, current approach also enables one to select the most suitable image depending on the size of the target.

B. PACT With In Vivo Mouse Model

In this *in vivo* experiment, all experimental procedures are complied with the rules on animal research and approved by the Animal Care and Use Committee of the University of Macau. Before the PA imaging, a nude mouse (male, six weeks, 50 g) was continuously anaesthetized with 2% isoflurane. Once the mouse was in fully anaesthetized state, the hair on the mouse head was shaved off properly by using a razor. Then, the mouse was secured by using a custom built fixture so that its head was aligned with the bottom hole of the water tank. In addition, a thin layer of transparent, ultrasound coupling gel was applied between the polyethylene film and the head of the mouse to enhance the coupling efficiency of the PA signal. In this paper, the *in vivo* experiment was performed on two mice having similar physiological status.

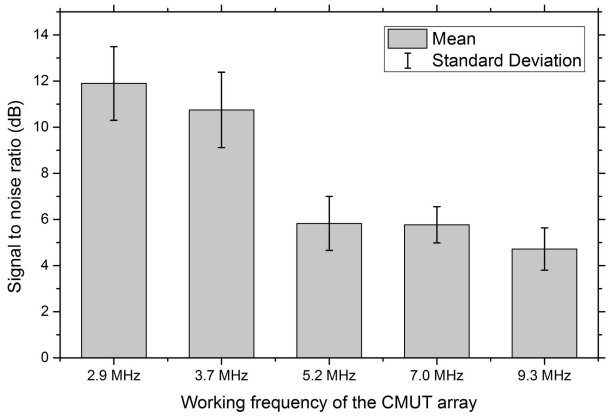

Fig. 9. Average SNR of the PACT images from the phantom experiment.

Fig. 10(a)–(e) shows the PACT images of the mouse brain obtained by the five center frequencies CMUT arrays. For comparison, the photograph of the mouse head used in the experiment is shown in Fig. 10(f). In Fig. 10(f), with the multiresolution capability of the PA imaging system enhanced by the proposed monolithic multiband CMUT arrays, different morphologies of the physiological structure of the brain can be found.

In general, from Fig. 10(f), the reconstructed images show increasing quality and detail of the brain with higher frequency detectors. To further explain the obtained PA images, the mouse brain and its major blood vasculatures beneath the skull were illustrated as shown in Fig. 10(g) [48], indicating the major vessels such as transverse sinus, superior sagittal sinus (SSS), inferior cerebral vein (ICV), superior cerebral veins (SCVs), and the olfactory lobe (OL) in the brain. In comparison, the reconstructed image from the PA signal of 2.9-MHz CMUT array can clearly show the shape of the brain and the large blood vessels—SSS and ICV. However, the detail structure of the brain is missing. With a higher frequency CMUT array −3.7-MHz CMUT array, the reconstructed image shows better structure of the brain and the OL of the brain is revealed. For the reconstructed image of 5.3-MHz CMUT array, the outer shape of the brain becomes blur; on the contrary, the structure of the blood vessels shows higher contrast. In particular, the SCV can be seen on the image but its dimension is not accurate. In comparison, the structure and dimension of the SCV on the reconstructed images from 7- and 9.3-MHz CMUT arrays are captured with high contrast, especially, in Fig. 10(e).

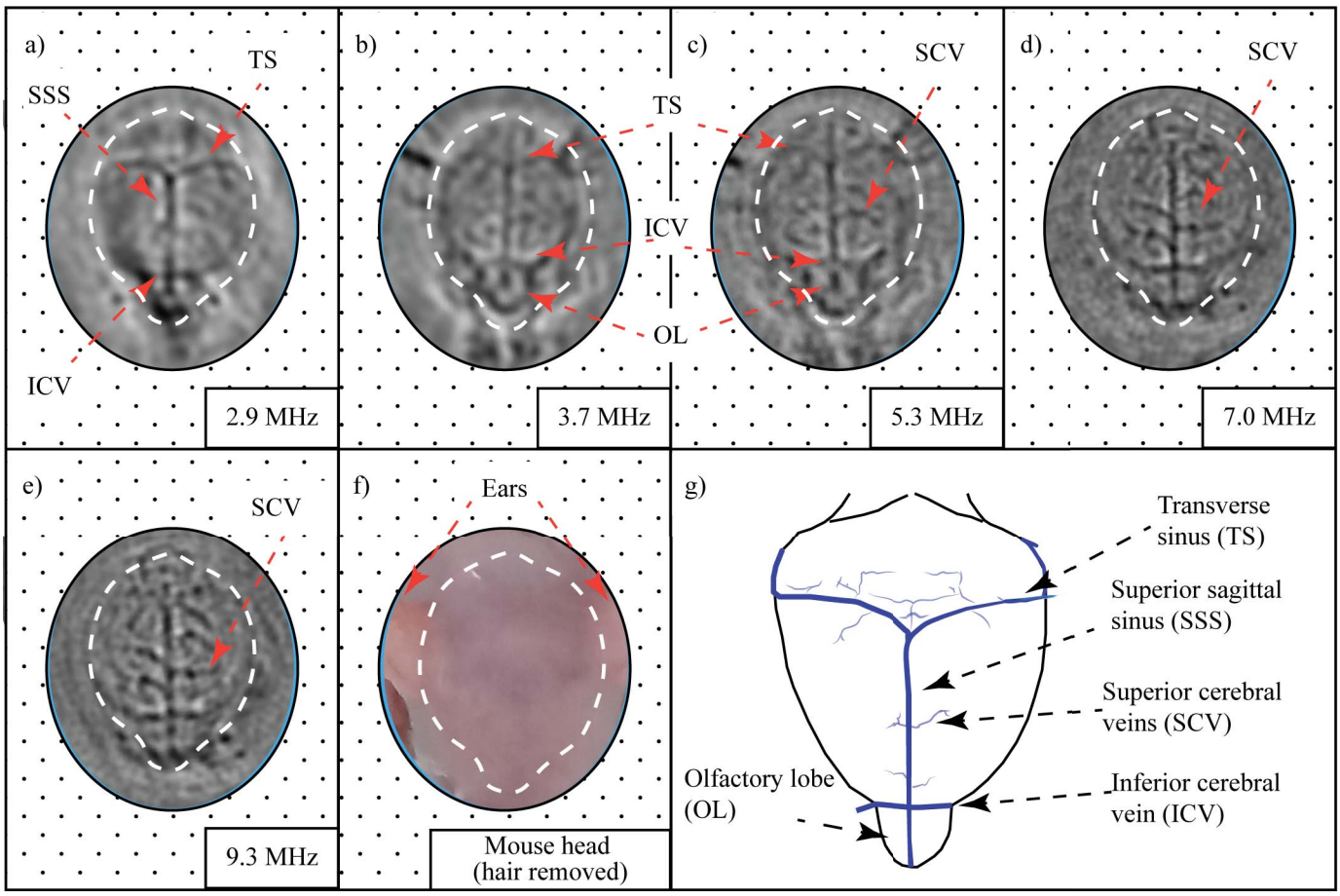

Fig. 10. (a)–(e) Reconstructed PACT images of the mouse model obtained by using the multiband CMUT arrays. (f) Photograph of the mouse head (hair removed) before experiment taken by a camera. (g) Illustration of the anatomy of the mouse brain showing the major blood vasculatures [48].

V. Conclusion

In this paper, multiband CMUT arrays were designed and fabricated for detecting the ultrasonic waves in the PACT. The proposed design integrated five CMUT arrays (centered frequencies: 2.9, 3.7, 5.3, 7, and 9.3 MHz) on a single die to provide a wide range coverage (~1.8–10.6 MHz) for acoustic signals generated by the PA effect. In addition to the basic pulse-echo measurement of the CMUT arrays, both phantom and *in vivo* biological experiments were performed with a custom built PACT imaging system to manifest the capabilities of the proposed designed for the multiscale PACT.

In conclusion, this paper reveals that the CMUT technology can provide a monolithic multiband solution for the multiscale PACT imaging system, which introduces the distinct advantages of CMUT to improve the performance of PACT imaging system. The experimental results also demonstrate that the current design can yield multiresolution tomographic images from various biological samples. In addition, the proposed methodology can ease the challenges of fabricating a wideband transducer for the reception of PA signal in PACT for biological tissue.

In the future, in order to improve the current PACT imaging system towards real-time, CMUT arrays with higher reception sensitivity can be built so as to reduce the lengthy PA signal acquisition time. Similarly, for small animal imaging application, a full-ring array [49], [50] or a spherical array [51] can be built with interlaced multiband CMUT elements to eliminate the mechanical scanning mechanism. Furthermore, more sophisticated reconstruction algorithm is going to develop to morph multiscale images into one composite image and passivation layer will be built to provide suitable intrinsic electrical insulation for the CMUTs.

Acknowledgment

The authors would like to express their appreciation for the assistance for the CMUT fabrication from the Nano Facility Center, National Chiao Tung University, Hsinchu, Taiwan, and the NEMS Research Center, National Taiwan University, Taipei, Taiwan.

References

[1] M. Xu and L. V. Wang, "Photoacoustic imaging in biomedicine," *Rev. Sci. Instrum.*, vol. 77, no. 4, p. 041101, 2006.

[2] J. Zhang, S. Yang, X. Ji, Q. Zhou, and D. Xing, "Characterization of lipid-rich aortic plaques by intravascular photoacoustic tomography: *Ex vivo* and *in vivo* validation in a rabbit atherosclerosis model with histologic correlation," *J. Amer. College Cardiol.*, vol. 64, no. 4, pp. 385–390, 2014.

[3] C. Li and L. V. Wang, "Photoacoustic tomography and sensing in biomedicine," *Phys. Med. Biol.*, vol. 54, no. 19, pp. R59–R97, 2009.

[4] V. G. Andreev, A. A. Karabutov, and A. A. Oraevsky, "Detection of ultrawide-band ultrasound pulses in optoacoustic tomography," *IEEE Trans. Ultrason., Ferroelect., Freq. Control*, vol. 50, no. 10, pp. 1383–1390, Oct. 2003.

[5] K. S. Valluru, B. K. Chinni, N. A. Rao, S. Bhatt, and V. S. Dogra, "Basics and clinical applications of photoacoustic imaging," *Ultrasound Clin.*, vol. 4, no. 3, pp. 403–429, 2009.

[6] A. H. Franzan, N. F. Leite, and L. C. M. Miranda, "Investigation of poling field effects on PVDF pyroelectric detectors: Photoacoustic thermal diffusivity measurements," *Appl. Phys. A, Solids Surf.*, vol. 50, no. 4, pp. 431–438, 1990.

[7] G. Ku, X. Wang, G. Stoica, and L. V. Wang, "Multiple-bandwidth photoacoustic tomography," *Phys. Med. Biol.*, vol. 49, no. 7, pp. 1329–1338, 2004.

[8] S. Vaithilingam *et al.*, "Three-dimensional photoacoustic imaging using a two-dimensional CMUT array," *IEEE Trans. Ultrason., Ferroelect., Freq. Control*, vol. 56, no. 11, pp. 2411–2419, Nov. 2009.

[9] P. C. Beard and T. N. Mills, "An optical detection system for biomedical photoacoustic imaging," *Proc. SPIE*, vol. 3916, pp. 34–42, Jan. 2001.

[10] T. Wang *et al.*, "All-optical photoacoustic microscopy based on plasmonic detection of broadband ultrasound," *Appl. Phys. Lett.*, vol. 107, no. 15, p. 153702, 2015.

[11] B. Dong, C. Sun, and H. F. Zhang, "Optical detection of ultrasound in photoacoustic imaging," *IEEE Trans. Biomed. Eng.*, vol. 64, no. 1, pp. 4–15, Jan. 2017.

[12] Y. Liu, Y. Wang, and Z. Yuan, "Dual-modality imaging of the human finger joint systems by using combined multispectral photoacoustic computed tomography and ultrasound computed tomography," *BioMed Res. Int.*, Sep. 2016, Art. no. 1453272.

[13] Y. Liu, D. Li, and Z. Yuan, "Photoacoustic tomography imaging of the adult zebrafish by using unfocused and focused high-frequency ultrasound transducers," *Appl. Sci.*, vol. 6, no. 12, p. 392, Nov. 2016.

[14] M. Xu and L. V. Wang, "Universal back-projection algorithm for photoacoustic computed tomography," *Phys. Rev. E, Stat. Phys. Plasmas Fluids Relat. Interdiscip. Top.*, vol. 71, no. 1, p. 016706, 2005.

[15] P. Burgholzer, G. J. Matt, M. Haltmeier, and G. Paltauf, "Exact and approximative imaging methods for photoacoustic tomography using an arbitrary detection surface," *Phys. Rev. E, Stat. Phys. Plasmas Fluids Relat. Interdiscip. Top.*, vol. 75, no. 4, p. 046706, 2007.

[16] J. Xia *et al.*, "Three-dimensional photoacoustic tomography based on the focal-line concept," *J. Biomed. Opt.*, vol. 16, no. 9, pp. 90503–90505, 2011.

[17] J. Qian, P. Stefanov, G. Uhlmann, and H. Zhao, "an efficient neumann series–based algorithm for thermoacoustic and photoacoustic tomography with variable sound speed," *SIAM J. Imag. Sci.*, vol. 4, no. 3, pp. 850–883, Jan. 2011.

[18] Z. Yuan and H. Jiang, "Quantitative photoacoustic tomography," *Philos. Trans. Roy. Soc., A, Math., physical, Eng. Sci.*, vol. 367, no. 1900, pp. 3043–3054, Aug. 2009.

[19] X. Cheng, J. Chen, and C. Li, "A miniature capacitive micromachined ultrasonic transducer array for minimally invasive photoacoustic imaging," *Microelectromech. Syst., J.*, vol. 19, no. 4, pp. 1002–1011, Aug. 2010.

[20] Ö. Oralkan *et al.*, "Capacitive micromachined ultrasonic transducers: Next-generation arrays for acoustic imaging?" *IEEE Trans. Ultrason., Ferroelect., Freq. Control*, vol. 49, no. 11, pp. 1596–1610, Nov. 2002.

[21] I. Ladabaum, X. Jin, H. T. Soh, A. Atalar, and B. T. Khuri-Yakub, "Surface micromachined capacitive ultrasonic transducers," *IEEE Trans. Ultrason., Ferroelect., Freq. Control*, vol. 45, no. 3, pp. 678–690, May 1998.

[22] F. L. Degertekin, R. O. Guldiken, and M. Karaman, "Annular-ring CMUT arrays for forward-looking IVUS: Transducer characterization and imaging," *IEEE Trans. Ultrason., Ferroelect., Freq. Control*, vol. 53, no. 2, pp. 474–482, Feb. 2006.

[23] I. O. Wygant, X. Zhuang, P. S. Kuo, D. T. Yeh, O. Oralkan, and B. T. Khuri-Yakub, "Photoacoustic imaging using a two-dimensional CMUT array," in *Proc. IEEE Ultrason. Symp.*, vol. 4. Sep. 2005, pp. 1921–1924.

[24] S. Vaithilingam *et al.*, "Tomographic photoacoustic imaging using capacitive micromachined ultrasonic transducer (CMUT) technology," in *Proc. IEEE Ultrason. Symp.*, Oct. 2006, pp. 397–400.

[25] S. Vaithilingam *et al.*, "Capacitive micromachined ultrasonic transducers (CMUTs) for photoacoustic imaging," *Proc. SPIE*, vol. 6086, pp. 608603–608611, Mar. 2006.

[26] R. K. W. Chee, A. Sampaleanu, D. Rishi, and R. J. Zemp, "Top orthogonal to bottom electrode (TOBE) 2-D CMUT arrays for 3-D photoacoustic imaging," *IEEE Trans. Ultrason., Ferroelect., Freq. Control*, vol. 61, no. 8, pp. 1393–1395, Aug. 2014.

[27] T.-J. Ma *et al.*, "3-D Deep penetration photoacoustic imaging with a 2-D CMUT array," in *Proc. IEEE Ultrason. Symp.*, Oct. 2010, pp. 375–377.

[28] S. Kothapalli, T.-J. Ma, S. Vaithilingam, O. Oralkan, B. T. Khuri-Yakub, and S. Sam Gambhir, "Deep tissue photoacoustic imaging using a miniaturized 2-D capacitive micromachined ultrasonic transducer array," *IEEE Trans. Biomed. Eng.*, vol. 59, no. 5, pp. 1199–1204, May 2012.

[29] J. Chen, M. Wang, J.-C. Cheng, Y.-H. Wang, P.-C. Li, and X. Cheng, "A photoacoustic imager with light illumination through an infrared-transparent silicon CMUT array," *IEEE Trans. Ultrason., Ferroelect., Freq. Control*, vol. 59, no. 4, pp. 766–775, Apr. 2012.

[30] R. K. W. Chee, P. Zhang, M. Maadi, and R. J. Zemp, "Multifrequency interlaced CMUTs for photoacoustic imaging," *IEEE Trans. Ultrason., Ferroelect., Freq. Control*, vol. 64, no. 2, pp. 391–401, Feb. 2017.

[31] J. Zhang *et al.*, "Development of a multi-band photoacoustic tomography imaging system based on a capacitive micromachined ultrasonic transducer array," *Appl. Opt.*, vol. 56, no. 14, pp. 4012–4018, 2017.

[32] Y. Asao *et al.*, "Photoacoustic mammography capable of simultaneously acquiring photoacoustic and ultrasound images," *J. Biomed. Opt.*, vol. 21, no. 11, p. 116009, 2016.

[33] M. A. Kalkhoran, F. Varray, and D. Vray, "Dual frequency band annular probe for volumetric pulse-echo optoacoustic imaging," *Phys. Procedia*, vol. 70, pp. 1104–1108, 2015.

[34] C. H. Sherman and J. L. Butler, *Transducers and Arrays for Underwater Sound*. New York, NY, USA: Springer, 2007.

[35] A. Novell, M. Legros, N. Felix, and A. Bouakaz, "Exploitation of capacitive micromachined transducers for nonlinear ultrasound imaging," *IEEE Trans. Ultrason., Ferroelect., Freq. Control*, vol. 56, no. 12, pp. 2733–2743, Dec. 2009.

[36] O. Warshavski *et al.*, "Experimental evaluation of cMUT and PZT transducers in receive only mode for photoacoustic imaging," *Proc. SPIE*, vol. 9708, p. 970830, Mar. 2016.

[37] X. Zhuang, "Capacitive micromachined ultrasonic transducers with through-wafer interconnects," Ph.D. dissertation, Stanford Univ., Stanford, CA, USA, 2008.

[38] C. Chang *et al.*, "Acoustic lens for capacitive micromachined ultrasonic transducers," *J. Micromech. Microeng.*, vol. 24, no. 8, p. 085007, 2014.

[39] G. G. Yaralioglu, A. S. Ergun, and B. T. Khuri-Yakub, "Finite-element analysis of capacitive micromachined ultrasonic transducers," *IEEE Trans. Ultrason., Ferroelect., Freq. Control*, vol. 52, no. 12, pp. 2185–2198, Dec. 2005.

[40] A. S. Erguri, Y. Huang, X. Zhuang, O. Oralkan, G. G. Yarahoglu, and B. T. Khuri-Yakub, "Capacitive micromachined ultrasonic transducers: Fabrication technology," *IEEE Trans. Ultrason., Ferroelect., Freq. Control*, vol. 52, no. 12, pp. 2242–2258, Dec. 2005.

[41] I. Ladabaum, P. Wagner, C. Zanelli, J. Mould, P. Reynolds, and G. Wojcik, "Silicon substrate ringing in microfabricated ultrasonic transducers," in *Proc. IEEE Ultrason. Symp.*, vol. 1. Oct. 2000, pp. 943–946.

[42] F. Etternavn, "Capacitive micromachined ultrasonic transducers: Acoustic challenges and proposed solutions," M.S. thesis, Norwegian Univ. Sci. Technol., Trondheim, Norway, 2012.

[43] M. Xu and L. V. Wang, "Analytic explanation of spatial resolution related to bandwidth and detector aperture size in thermoacoustic or photoacoustic reconstruction," *Phys. Rev. E, Stat. Phys. Plasmas Fluids Relat. Interdiscip. Top.*, vol. 67, no. 5, pp. 056605-1–056605-15, 2003.

[44] *American National Standard for the Safe Use of Lasers*, Standard ANSI Z136.1-2007, American National Standards Institute, 2007.

[45] S. T. Flock, S. L. Jacques, B. C. Wilson, W. M. Star, and M. J. C. van Gemert, "Optical properties of intralipid: A phantom medium for light propagation studies," *Lasers Surgery Med.*, vol. 12, no. 5, pp. 510–519, 1992.

[46] L. E. Kinsler, A. R. Frey, A. B. Coppens, and J. V. Sanders, *Fundamentals of Acoustics*, 4th ed. Hoboken, NJ, USA: Wiley, 1999.

[47] R. G. Maev, *Acoustic Microscopy: Fundamentals and Applications*. Hoboken, NJ, USA: Wiley, 2008.

[48] H. J. Hedrich, *The Laboratory Mouse*. San Francisco, CA, USA: Academic, 2012.

[49] J. Gamelin *et al.*, "A real-time photoacoustic tomography system for small animals," *Opt. Exp.*, vol. 17, no. 13, pp. 10489–10498, 2009.

[50] C. Li, A. Aguirre, J. Gamelin, A. Maurudis, Q. Zhu, and L. V. Wang, "Real-time photoacoustic tomography of cortical hemodynamics in small animals," *J. Biomed. Opt.*, vol. 15, no. 1, p. 010509, 2010.

[51] B. Wang *et al.*, "Photoacoustic tomography system for noninvasive real-time three-dimensional imaging of epilepsy," *Biomed. Opt. Exp.*, vol. 3, no. 6, pp. 1427–1432, 2012.

Sio Hang Pun (S'11–A'12–M'12) received the master's degree in computer and electrical program from the University of Porto, Porto, Portugal, in 1999, and the Ph.D. degree in electrical and electronics engineering from the University of Macau, Macau, China, in 2012.

Since 2012, he has been an Assistant Professor with the State Key Laboratory of Analog and Mixed-Signal VLSI, University of Macau. His current research interests include biomedical electronic circuits, miniaturized sensors for biomedical applications, and human body communication.

Yuanyu Yu (S'15–M'17) received the B.S. degree in biomedical engineering and the M.S. degree in measuring and testing technologies and instruments from the University of Electronic Science and Technology of China, Chengdu, China, in 2000 and 2005, respectively, and the Ph.D. degree in electrical and electronics engineering from the University of Macau, Macau, China, in 2017.

From 2012 to 2017, he was a Research Fellow with the State Key Laboratory of Analog and Mixed-Signal VLSI, University of Macau. Since 2017, he has been an Assistant Professor with the School of Information Engineering, Lingnan Normal University, Zhanjiang, China. His research interests include the design, modeling, and fabrication of capacitive micromachined ultrasonic transducers.

Jian Zhang received the Ph.D. degree from the MOE Key Laboratory of Laser Life Science, Institute of Laser Life Science, South China Normal University, Guangzhou, China, in 2014.

From 2014 to 2016, he was a Post-Doctoral Research Staff member with the University of Macau. He is currently the Leader of the Biomedical Photonics Lab, Guangzhou Medical University, Guangzhou. His research mainly focuses on laser-tissue interaction, photoacoustic imaging, optical coherence tomography, and molecular imaging.

Jiujiang Wang (S'14) received the B.S. degree in microelectronic circuits and systems from the Beijing Institute of Technology, Beijing, China, in 1991, and the M.S. degree in semiconductor devices and microelectronics from the Institute of Semiconductors, Chinese Academy of Sciences, Beijing, in 1994. He is currently pursuing the Ph.D. degree in electrical and computer engineering with the University of Macau, Macau, China.

He was a System Design Engineer with IC company, Zhuhai, China. His current research interests include the modeling and fabrication of capacitive micromachined ultrasonic transducer devices.

Ching-Hsiang Cheng (M'07) received the B.S. degree in mechanical engineering from National Taiwan University, Taipei, Taiwan, in 1993, the master's degrees in mechanical, electrical engineering, and science from Cornell University, Ithaca, NY, USA, in 1996, 1997, and 1998, respectively, and the Ph.D. degree in electrical engineering from Stanford University, Stanford, CA, USA, in 2005.

After completing his post-doctoral research with the Department of Mechanical Engineering at Stanford, he joined the Mechanical and Systems Research Laboratories, Industrial Technology Research Institute, Hsinchu, Taiwan, as a Researcher and became a Project Leader. In 2006, he joined the Research Institute of Innovative Products and Technologies, The Hong Kong Polytechnic University (PolyU), Hong Kong, as an Assistant Professor and a Research Engineer. In 2010, he joined the Department of Industrial and Systems Engineering, PolyU, as an Assistant Professor. Since 2017, he has been with the School of Automotive Engineering, Wuhan University of Technology, Wuhan, China, as an Associate Professor. His research interests include capacitive micromachined ultrasonic transducers, energy storage devices, shear and normal force sensors, large strain and tactile sensors, solar cells, microvalves and micropumps, gas sensors, electrical through-wafer interconnects, nanotechnology, and microelectromechanical systems.

Kin Fong Lei (M'13–SM'17) received the M.Phil. and Ph.D. degrees from The Chinese University of Hong Kong, Hong Kong, in 2000 and 2005, respectively.

In 2006, he joined the University of Western Ontario, London, ON, Canada, as a Post-Doctoral Fellow. From 2007 to 2010, he was a Lecturer with The Hong Kong Polytechnic University, Hong Kong. In 2010, he joined Chang Gung University, Taoyuan, Taiwan, as an Assistant Professor and was promoted to an Associate Professor in 2014. He has authored over 100 academic papers and was invited to contribute in eight books/book chapters.

Dr. Lei also served as a Technical Program Committee Member for the IEEE conferences for MEMS/microfluidics researchers, i.e., IEEE-NEMS 2014 (Hawaii), 2017 (Los Angeles), and 2018 (Singapore). His current research interests include biomicrofluidics, biosensing, rapid diagnostics, and cancer biology.

Zhen Yuan (M'14) received the Ph.D. degree in mechanical engineering from the University of Science and Technology of China, Hefei, China, in 2002.

From 2002 to 2007, he received several post-doctoral trainings in different institutes including the National University of Singapore, Singapore, from 2002 to 2004, Clemson University, Clemson, SC, USA, in 2005, and the University of Florida from 2005 to 2007. From 2007 to 2012, he was a Research Assistant Professor with the University of Florida, Gainesville, FL, USA. From 2012 to 2013, he was a Clinical Assistant Professor with the Arizona State University, Tempe, AZ, USA. He is the Director of Bioimaging Core with the Faculty of Health Sciences, University of Macau (UM), Macau, China. He is currently an Associate Professor with UM. Since 2013, he has been an Assistant Professor with UM and has been promoted to a tenured Associate Professor, effective since 2017. His academic investigation is focused on cutting-edge research and development in biomedical optics and optical imaging. He has achieved national and international recognition through over 100 publications in high-ranked journals in his field, as the Principal or Co-Investigator for the above research activities.

Dr. Yuan was selected to be an active reviewer for over 50 top journals. He is a Senior Member of OSA and SPIE.

Peng Un Mak (S'88–M'97–SM'11) received the B.Sc. degree in electrical engineering from National Taiwan University, Taipei, Taiwan, and the M.Sc. and Ph.D. degrees in electrical engineering from Michigan State University, East Lansing, MI, USA.

Since 1997, he has been the first Assistant Professor with the Department of Electrical and Computer Engineering, University of Macau, Macau, China. He has authored or co-authored over 140 peer-reviewed technical publications (journals, book chapters, and conference proceedings). He has performed research in biosignal extraction and processing, bioelectromagnetism, human body communication, and body sensor network.

Dr. Mak is also a Life Member of Phi Kappa Phi and an Invited Member of Eta Kappa Nu (currently IEEE-HKN).